

STUDY ON THE HIGH PRECISION RELATIVE ORBIT CONTROL STRATEGY FOR FFAST MISSION

Toshinori Ikenaga⁽¹⁾, Isao Kawano⁽²⁾, Hiroshi Tsunemi⁽³⁾ and Nobuaki Ishii⁽⁴⁾

⁽¹⁾JAXA/ARDD, 2-1-1, Sengen, Tsukuba, Ibaraki, Japan, +81.50.3362.4109,
ikenaga.toshinori@jaxa.jp

⁽²⁾JAXA/ARDD, 2-1-1, Sengen, Tsukuba, Ibaraki, Japan, +81.50.3362.4145,
kawano.isao@jaxa.jp

⁽³⁾Osaka University, 1-1, Machikaneyama-machi, Toyonaka, Osaka, Japan, +81.6.6850.5477,
tsunemi@ess.sci.osaka-u.ac.jp

⁽⁴⁾JAXA/ISAS, 3-1-1, Yoshinodai, Chuo-ku, Sagamihara, Kanagawa, Japan, +81.50.3362.3591,
ishii.nobuaki@jaxa.jp

Abstract: Japan Aerospace Exploration Agency, JAXA, is now planning the Formation Flight All-Sky Telescope, FFAST, mission that covers a large sky area in relatively high energy X-ray. It consists of two 300 kg class small satellites i.e. one is an X-ray telescope satellite and the other is a detector satellite. The focusing distance is 20 m, which is quite difficult for one satellite to realize, however precisely controlled formation flight enables to construct the long focus X-ray telescope system. The relative distance between the two satellites is required to be maintained within $20\text{ m} \pm 5\text{ cm}$. For this purpose, a high precision relative circular orbit control algorithm applicable to FFAST mission is constructed and proposed in this paper. The feasibility of the algorithm is evaluated through some cases of simulations under “real-world” dynamics i.e. perturbed forces caused by the Earth’s gravitational potential, the air drag, the solar radiation pressure and the disturbing forces by the other celestial bodies.

Keywords: FFAST, Formation Flight, Relative Circular Orbit.

1. Introduction

The primary aim of this work is to construct the high precision formation flight control algorithm applicable to the Formation Flight All-Sky Telescope, FFAST, mission[1]. FFAST is a long focus X-ray telescope system that covers a large sky area in relatively high energy X-ray. It consists of two 300 kg small satellites i.e. one is an X-ray telescope satellite and the other is a detector satellite. The focusing distance is 20 m, which is quite difficult for one satellite to realize, however precisely controlled formation flight enables to construct the long focus X-ray telescope system. The relative distance between the two satellites is required to be maintained within $20\text{ m} \pm 5\text{ cm}$. For this purpose, a high precision relative circular orbit control algorithm is constructed and proposed in this paper. The feasibility of the algorithm is evaluated through some cases of simulations under “real-world” dynamics i.e. perturbed forces caused by the Earth’s gravitational potential, the air drag, the solar radiation pressure and the disturbing forces by the other celestial bodies.

2. Relative Circular Orbit for FFAST Mission

In this study, a relative circular orbit, RCO, in which the detector satellite (Chaser) flies near circularly around the telescope satellite (Target), is employed to compose the long focus X-ray telescope system. Figure 2 shows the diagram of RCO described in Target-centered rotational coordinate system i.e. Hill frame. In an assumption of the two-body problem, a RCO is realized by the combination of 2:1 in-plane motion and $\sqrt{3}$ out-of-plane motion in Hill frame.

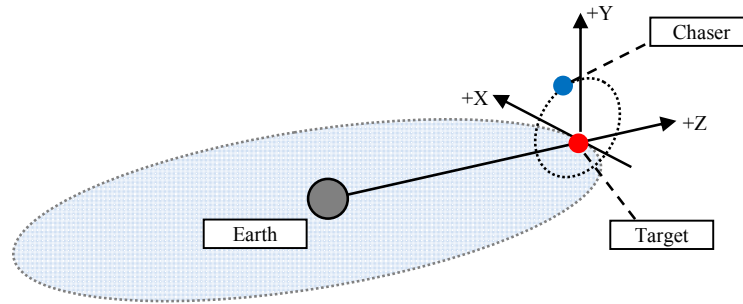


Figure 2. Diagram of RCO

3. Force Model and Coordinate System

3.1. Force Model

In this study, the Earth's gravitational potential, the air drag, the solar radiation pressure and the disturbing forces by the Sun and Moon are considered. Table 3-1-1 summarizes the detail of the perturbations.

Table 3-1-1. Perturbations

Terms	Detail
Geo-potential model	WGS84EGM96 model (36 x 36)
Atmosphere model	NRLMSISE-00 model [3] MSAFE 95% model (2012/Sep, published)
Solar Radiation Pressure	Seasonal changes of Solar Flux considered Eclipses considered
Third-Body Perturbations	Sun and Moon (orbits determined by DE405)

To evaluate the feasibility of the relative orbit control strategy constructed in this study, the initial epoch of the simulation is determined in 2024 in which the solar activity is maximum i.e. the air drag is maximum, according to the current monthly report (2012/Sep, published) based on the Marshall Solar Activity Future Estimation, MSAFE, model [4]. Figure 3-1-1 shows the future estimation of the 10.7 cm Solar Flux ($F_{10.7}$) and the Geomagnetic Index (A_p).

The relative orbit changes by the above-mentioned perturbations. Figure 3-1-2 shows the relative range deviation by each perturbation. As shown in Figure 3-1-2, the dominant influence to the

relative range deviation between the two satellites is the air drag. The relative range deviation by the air drag after 7-day free flight is about 770 m while the deviation by the solar radiation pressure, SRP, which is the second largest deviation, is about 25 m.

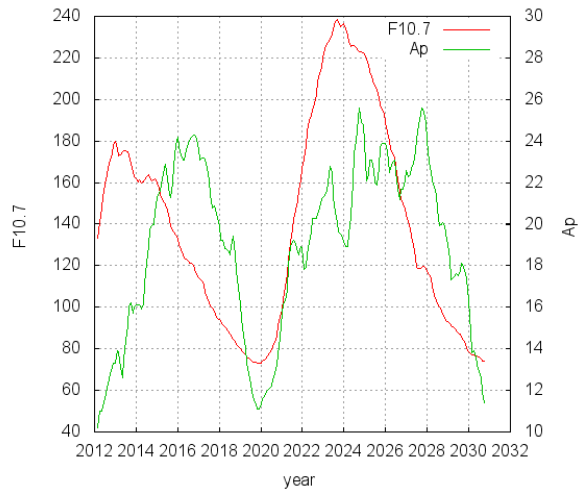


Figure 3-1-1. Future Estimation of $F_{10.7}$ and A_p based on 2012/Sep report published by Marshall Space Flight Center

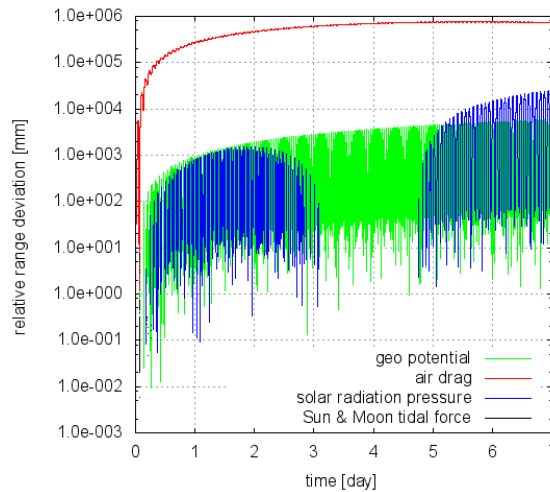


Figure 3-1-2. Variation of Relative Range Deviation by Perturbations

3.2. Coordinate System

In this study, three coordinate systems i.e. the mean equator and equinox of J2000 designated as Earth-Centered Inertial, ECI, system, Hill coordinate system (“H” system) and the spacecraft’s

(S/C) body-fixed coordinate system (“B” system) are handled. The definitions of each coordinate system of this study are shown in the following sections.

Hill coordinate system (“H” system)

Each axis of Hill coordinate system of this study are defined as the following;

$$\vec{X}_H = \vec{Y}_H \times \vec{Z}_H, \vec{Y}_H = \frac{\vec{r}_{ECI} \times \vec{v}_{ECI}}{|\vec{r}_{ECI} \times \vec{v}_{ECI}|}, \vec{Z}_H = \vec{r}_{ECI} / |\vec{r}_{ECI}| \quad (3-2-1)$$

where \vec{r}_{ECI} , \vec{v}_{ECI} are the range and velocity vectors of the Target satellite.

S/C body-fixed coordinate system (“B” system)

Each axis of S/C body-fixed coordinate system of this study are defined as the following;

$$\vec{X}_B = \vec{r}_{C/T} / |\vec{r}_{C/T}|, \vec{Y}_B = \frac{\vec{r}_S \times \vec{r}_{C/T}}{|\vec{r}_S \times \vec{r}_{C/T}|}, \vec{Z}_B = \vec{X}_B \times \vec{Y}_B \quad (3-2-2)$$

where \vec{r}_s is the sun vector with respect to the S/C, and $\vec{r}_{C/T}$ is the direction vector from Target to Chaser satellites.

4. High Precision Relative Orbit Control Law

4.1. Relative Circular Orbit Keeping Algorithm

Figure 4-1-1 shows the diagram of the relative circular orbit keeping.

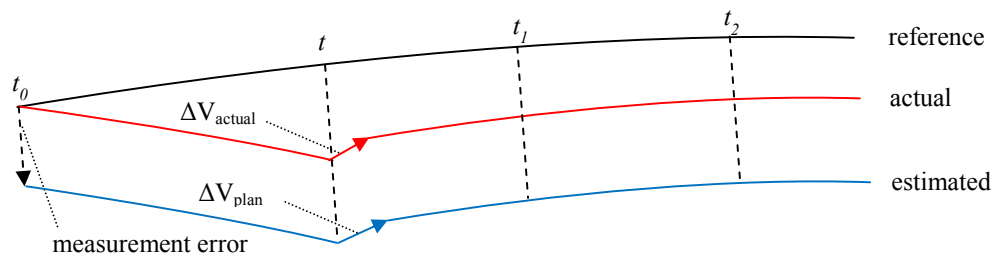


Figure 4-1-1. Diagram of Relative Circular Orbit Keeping Control Law

This study deals with three relative orbits: a “reference” orbit which is a perfectly relative circular orbit, an “actual” orbit in which the spacecraft flies, and an “estimated” orbit which is determined via extended Kalman filtering method based on the relative range data measured by FF Image Navigation Equipment, FINE. The state estimation filtering algorithm is explained in

the next section. Note that only Chaser is controlled and no state error of Target's orbit is considered in this study.

The reference relative orbit is a circular orbit with the angular velocity, ω_{ref} . The angular velocity is described as the following;

$$\omega_{ref} = (1 + k) \sqrt{\frac{\mu_E}{a_T^3}} \quad (4-1-1)$$

where μ_E is the Earth's gravitational constant, a_T is the semi-major axis of Target satellite. The constant k has sensitivity to the total amount of the corrective control maneuvers. The value of k is set to "0.0025" in this study, which is almost equal to the secular variation of the mean argument of latitude by J_2 perturbation i.e. "0.0027" [5].

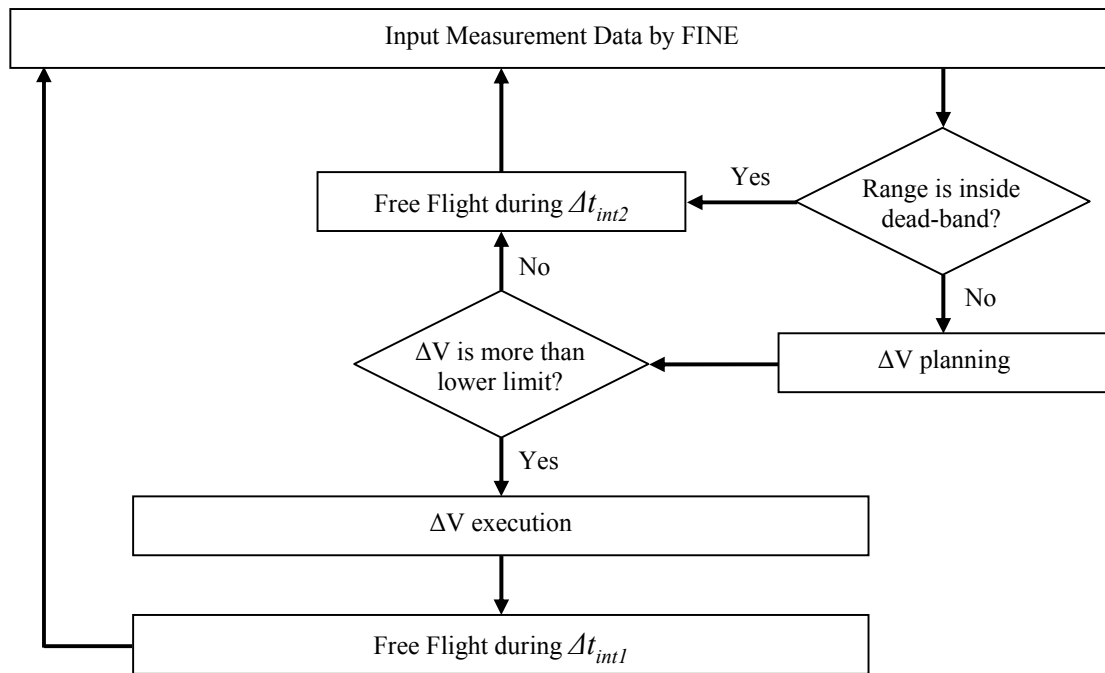


Figure 4-1-2. Flow-Chart of Relative Circular Orbit Keeping Algorithm

The relative circular orbit keeping algorithm is constructed with reference to the paper written by K. C. Howell et al. [1993] [6]. This algorithm minimizes the sum of a corrective maneuver and deviations between the reference and estimated orbits at two target epochs (t_1 and t_2) in ECI frame.

When we divide the 6 x 6 state transition matrix, STM, evaluated from initial epoch t_0 to certain time t ($t > t_0$) in ECI frame by four 3 x 3 submatrices as shown in the following;

$$\Phi(t, t_0) = \begin{bmatrix} A_{tt_0} & B_{tt_0} \\ C_{tt_0} & D_{tt_0} \end{bmatrix} \quad (4-1-2)$$

The deviation between the reference and estimated orbits at epoch t_i ($t_i > t_0$) is evaluated as the following;

$$\vec{m}_{t_i} \cong B_{t_i t_0} \vec{e}(t_0) + B_{t_i t_0} \Delta \vec{V}(t_0) + A_{t_i t_0} \vec{p}(t_0) \quad (4-1-3)$$

The three vectors $\vec{p}(t_0)$, $\vec{e}(t_0)$ and $\Delta \vec{V}(t_0)$ are the position deviation, velocity deviation at epoch t_0 , and the corrective control maneuver executed at epoch t ($t_i > t > t_0$), respectively. The optimal corrective control maneuver is computed by minimizing the cost function defined as the following;

$$J[\vec{p}, \vec{e}, \Delta \vec{V}] = \Delta \vec{V}^T Q \Delta \vec{V} + \vec{m}_{t_1}^T R \vec{m}_{t_1} + \vec{m}_{t_2}^T S \vec{m}_{t_2} \quad (4-1-4)$$

where the three matrices Q , R and S are 3 x 3 weighting diagonal matrices.

The corrective control maneuver is planned if the deviation between the reference and the relative range measured by FINE is outside the pre-determined deviation (dead-band) i.e. 40 mm in the line of sight, LOS, direction and 1 mm in the orthogonal directions. The corrective maneuver is executed if the planned ΔV is more than the lower limit. Note that it is assumed corrective ΔV s can be applied in all directions in this study however the applied ΔV s have maneuver control errors i.e. 5 % ΔV scalar error (1σ) and 0.17° attitude error (1σ). Once a corrective ΔV is executed, the spacecrafts fly freely during Δt_{int1} . If corrective ΔV is not executed, the next ΔV is planned after Δt_{int2} . Figure 4-1-2 shows the flow-chart of this algorithm and Table 4-1-1 describes parameters of this algorithm.

Table 4-1-1. Parameters Input to Relative Circular Orbit Keeping Algorithm

Terms	Detail
Δt_{int1}	Time interval of ΔV planning.
Δt_{int2}	Time interval executing the next ΔV in case planned ΔV is not executed.
Δt_1	Time interval between ΔV execution time and target epoch t_1 .
Δt_2	Time interval between ΔV execution time and target epoch t_2 .
ΔV_{min}	Minimum amount of ΔV .

4.2. State Estimation Filtering Algorithm

As mentioned in the previous section, the estimated relative orbit is determined via extended Kalman filtering based on the relative range measured by FINE.

Table 4-2-1 shows the measurement error of FINE.

Table 4-2-1. Measurement Error of FINE Sensor

Terms	Bias Error	Random Error (1σ)
LOS direction	10.0 mm	3.0 mm
LOS orthogonal direction	1.0 mm	0.2 mm

Figure 4-2-1 shows the diagram of the state estimation filtering. The \bar{X}_k is 6-dimensional state vector at epoch t_k , Φ_{k+1} is the state transition matrix from epochs t_k to t_{k+1} , P_k is the covariance matrix at epoch t_k , K_{k+1} is the Kalman gain matrix and \bar{r}_{FINE} is 3-dimensional relative range vector measured by FINE.

The covariance matrix, P_k , propagated from epochs t_k to t_{k+1} is described as the following;

$$\bar{P}_{k+1} = \Phi_{k+1} P_k \Phi_{k+1}^T + Q \quad (4-2-1)$$

The matrix, Q , appearing in the equation 4-2-1 is a process noise matrix, which is described as the following in this study [8];

$$Q = \begin{bmatrix} \frac{1}{3} S_p \Delta t^3 I_{3 \times 3} & \frac{1}{2} S_p \Delta t^2 I_{3 \times 3} \\ \frac{1}{2} S_p \Delta t^2 I_{3 \times 3} & S_p \Delta t I_{3 \times 3} \end{bmatrix} \quad (4-2-2)$$

where S_p is the spectral amplitude associated with the white noise driving function, Δt is the difference between the epochs t_k and t_{k+1} , and $I_{3 \times 3}$ is 3 x 3 identity matrix.

The Kalman gain matrix, K_{k+1} , is computed as the following formula;

$$K_{k+1} = \bar{P}_{k+1} H^T \left[H \bar{P}_{k+1} H^T + R \right]^{-1} \quad (4-2-3)$$

where R is an observation noise matrix which corresponds to the sensor's noise i.e. FINE measurement noise, and H is an observation matrix which describes the relationship between the

state parameter, \bar{X} , and the observation values, \bar{r}_{FINE} . The matrix H for this study is described as the following;

$$H = \begin{bmatrix} \frac{\partial \bar{r}}{\partial \bar{r}} & \frac{\partial \bar{r}}{\partial \bar{v}} \\ \frac{\partial \bar{v}}{\partial \bar{r}} & \frac{\partial \bar{v}}{\partial \bar{v}} \end{bmatrix} = \begin{bmatrix} I_{3 \times 3} & O_{3 \times 3} \end{bmatrix} \quad (4-2-4)$$

where $O_{3 \times 3}$ is 3 x 3 zero matrix.

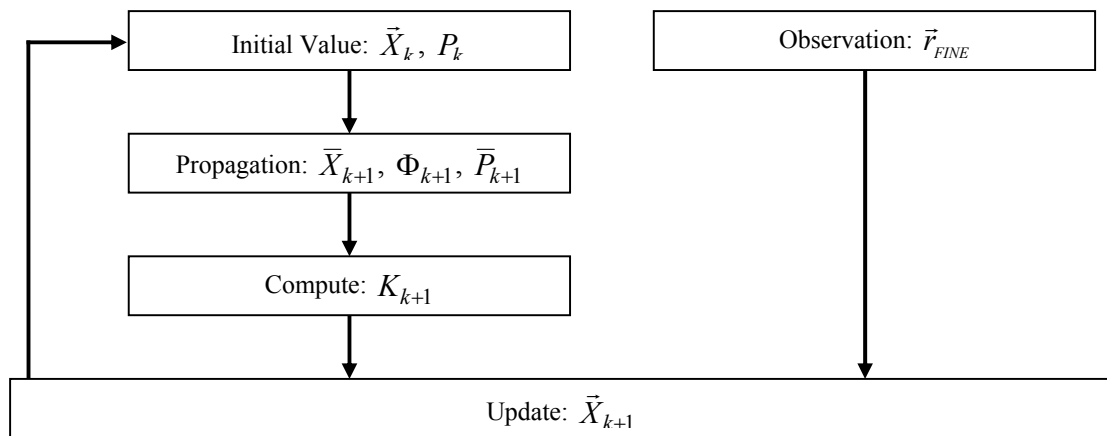


Figure 4-2-1. Diagram of State Estimation Filtering

Note that the force model of the estimation filter is assumed as same as “actual” force model in this study. Practically, the force model for on-board computation must be much simpler because of the limited recourses hence further research for this point is necessary.

5. Relative Circular Orbit Control Simulation

5.1. Configuration

The initial orbital elements of Target and Chaser in the simulation are summarised in Table 5-1-1.

Table 5-1-1. Initial Orbital Elements

a) Target		
Term	Unit	Value
Semi-major axis	km	6928 (Alt. 550.0)
Eccentricity	--	0.003
Inclination	deg	31.0
RAAN	deg	0.0
Argument of Perigee	deg	0.0
True Anomaly	deg	0.0

b) Chaser (Hill frame)

Term	Unit	Value
R_x	m	20.0
R_y	m	0.0
R_z	m	0.0
V_x	m/s	0.0
V_y	m/s	1.896e-2
V_z	m/s	1.095e-2

In this study, it is assumed that the two satellites are launched to the East from Japanese launch site by JAXA's epsilon rocket which is next Japanese solid propellant rocket under development. The eccentricity of Target is determined based on the injection error of the epsilon rocket i.e. ± 20 km.

Table 5-1-2 shows the specification of the spacecrafts for this study. Note that the vector normal to maximum area plane i.e. SAP of each spacecraft corresponds to Z axis of each body-fixed frame (See Sec. 3-2).

Table 5-1-2. Specification of Spacecrafts

Term	Unit	Target	Chaser
Mass	kg	300.0	300.0
Maximum Area	m ²	4.8	7.3
C_R	--		1.3
C_D	--		2.2

5.2. State Estimation

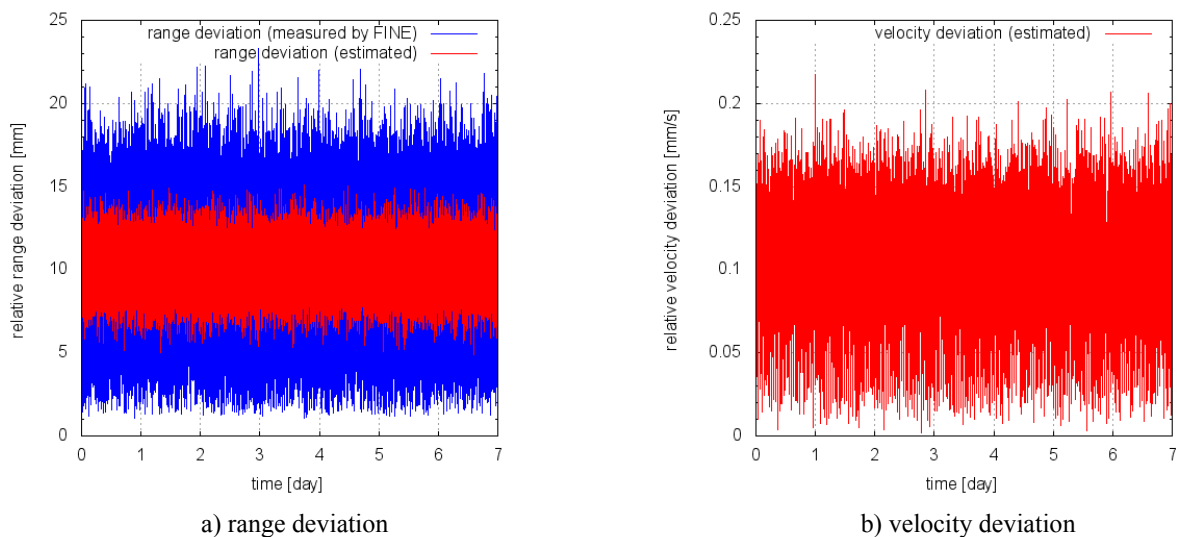


Figure 5-2-1. Range & Velocity Deviations between Actual and Estimated Orbits

This section describes the results of the state estimation filtering. Figure 5-2-1 shows the relative range and velocity deviations between the actual and estimated orbits. As mentioned FINE measures only the relative range.

Table 5-2-1 summarises the result of the state estimation. μ and σ are the mean value and standard deviation of the relative range deviation estimated by the filter. The values in the parenthesis are the deviation based on the measurement range by FINE. The mean deviation can not be removed because it is determined by the bias error. The mean and standard deviation of the velocity are 0.10 and 0.03 mm/s, respectively, which are small enough for this study.

Table 5-2-1. Deviation between Actual and Estimated Orbits

Term	Unit	μ	σ
Range	mm	10.11 (10.12)	1.29 (2.96)
Velocity	mm/s	0.10	0.03

5.3. Simulation

Table 5-3-1 summarises the parameters input to the relative circular orbit keeping algorithm for this study. The amount of minimum ΔV , $1.0e-4$ m/s, is equal to 30 msec impulse bit of a 1N thruster. The duration of the simulation is 7 days.

Table 5-3-1. Parameters

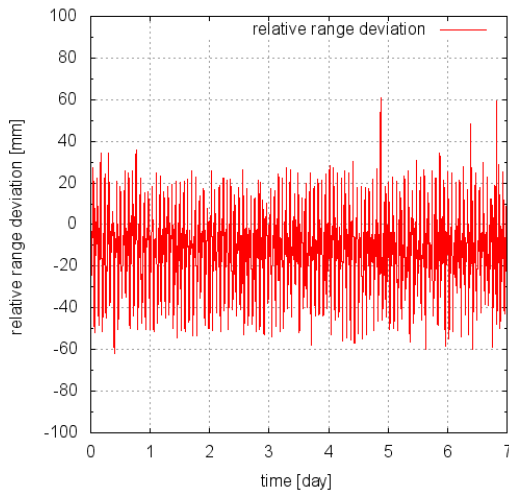
Term	Unit	Value
Δt_{int1}	sec	90.0
Δt_{int2}	sec	10.0
Δt_1	sec	180.0
Δt_2	sec	210.0
ΔV_{min}	m/s	$1.0e-4$

Figure 5-3-1 shows the relative range and position deviation in LOS and LOS orthogonal directions. “LOS orthogonal 1” in Figure 5-3-1 b) is the velocity direction and “LOS orthogonal 2” is the angular velocity direction of the reference relative orbit in Hill frame. The position deviation of each direction varies in almost same range however the deviation in “LOS orthogonal 2” direction is somehow narrow. The relative range deviations with reference to 20 m are almost in the range from -50 mm to 50 mm. Table 5-3-2 summarises the deviations.

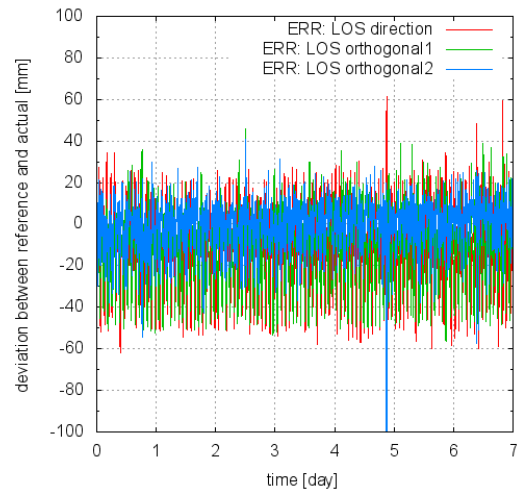
Table 5-3-2. Relative Range Deviation with reference to 20 m

Term	Unit	Value
Mean Deviation	mm	-12.15
Standard Deviation	mm	18.03

From the simulation results, it is concluded that 98 % of whole data is within the required relative range i.e. $20 \text{ m} \pm 5 \text{ cm}$. The total corrective ΔV s for 7-day relative orbit keeping is 0.34 m/s, which is 17.50 m/s/yr. If we assume the specific impulse of the on-board thruster as 200 sec, the mass of propellant for 1 year orbit keeping is about 2.7 kg/yr.



a) relative range deviation



b) deviation in LOS and LOS orthogonal direction

Figure 5-3-1. Relative Position Deviation between Reference and Actual Orbits

6. Conclusion

In this study, the high precision relative orbit control strategy was constructed and the feasibility of the algorithm was evaluated through a simulation under “real-world” dynamics considering the Earth’s geo-potential, air drag, solar radiation pressure and tidal forces by Sun and Moon. Upon the simulation results, it was revealed that the relative range can be maintained within the required relative range i.e. $20\text{ m} \pm 5\text{ cm}$ in 98 % possibility. The total corrective ΔV s for 1-year relative orbit keeping is 17.5 m/s, which equals to 2.7 kg propellant mass with 200 sec specific impulse.

For future works, the following things are anticipated;

- 1) Consideration of the orbit estimation errors of Target.
- 2) Consideration of the attitude constraints, thruster allocation and thruster control scheme. The misalignment between the spacecraft mass center and thrust vector directions should be considered.
- 3) Construction of the force model for on-board computation. Also, further study on the relative orbit keeping algorithm to decrease the computation load will be necessary for the development of the on-board algorithm.

Acknowledgments

I would like to express my great appreciation to Dr. Masayoshi Utashima, for his valuable advices and continuous support. His insightful comments based on his professional carrier and vast knowledge always inspired me in doing the research.

7. References

- [1] Tsunemi, H. Hayashida, K. Kunieda, H. Ogasaka, Y. Itoh, M. Ozaki, M. Kawano, I. and FFAST team. "High-energy X-ray Sky Observation by the Formation Flight All Sky Telescope", Trans. JSASS Aerospace Tech. Japan, Vol. 8, No. ists27, pp. To_4_7-To_4_12, 2010
- [2] Mitani, S. Yamamoto, T. Kawano, I. Sakai, S. Tsunemi, H. and FFAST team. "FFAST: Formation Flight All Sky Telescope, Formation Flight System Analysis and Design", Trans. JSASS Aerospace Tech. Japan, Vol. 8, No. ists27, pp. Td_7-Td_15, 2010
- [3] Picone, J.M. Hedin, A.E. and Drob, D.P. "NRLMSISE-00 empirical model of the atmosphere: Statistical comparisons and scientific issues", JOURNAL OF GEOPHYSICAL RESEARCH, Vol.107, No.A12, 1468, 2002
- [4] Niehuss, K.O. Euler Jr, H.C. and Vaughan, W.W. "Statistical Technique for Intermediate and Long-Range Estimation of 13-Month Smoothed Solar Flux and Geomagnetic Index", NASA Technical Memorandum 4759, Sep 1996
- [5] Utashima, M. Hirota, M. and Tanaka, A. "Dynamics for Sun Synchronous Near Recurrent Orbit (Revised Edition)" NASDA, Tracking and Control Center in Tsukuba Space Center, TK-M15101, 1986 (in Japanese)
- [6] Howell, K.C. Pernicka, H.J. "Stationkeeping Method for Libration Point Trajectories", JOURNAL OF GUIDANCE, CONTROL and DYNAMICS, January-February, vol.16, No.1, 1993
- [7] Ikenaga, T. and Utashima, M. "Study on the Stationkeeping Strategy for the Libration Point Mission", ISTS28, 2011
- [8] Brown, R.G and Hwang, P.Y.C. "Introduction to Random Signals and Applied Kalman Filtering", John Wiley & Sons, Third Edition, 1997
- [9] Imamura, S. and Utashima, M. "Initial Orbit Control of SLATS using Atmospheric Drag", ISTS28, 2011